Journal of Catalysis **182,** 56–69 (1999)
Article ID jcat.1998.2321, available online at http://www.idealibrary.com on IDEAL®

Redox Behavior of High-Surface-Area Rh-, Pt-, and Pd-Loaded $Ce_{0.5}Zr_{0.5}O_2$ Mixed Oxide

Paolo Fornasiero, Jan Kašpar,[1] Valter Sergo,* and Mauro Graziani

*Dipartimento di Scienze Chimiche, Università di Trieste, Via Giorgieri 1, 34127 Trieste, Italy; and *Dipartimento di Ingegneria dei Materiali e Chimica Applicata, Università di Trieste, Via A. Valerio 2, 34127 Trieste, Italy*

Received May 12, 1998; revised September 11, 1998; accepted November 2, 1998

The temperature programmed reduction, oxygen uptake, and surface area stability of high-surface-area Rh-, Pt-, and Pd-loaded $Ce_{0.5}Zr_{0.5}O_2$ solid solution have been investigated. It is observed that the presence of the noble metal strongly favors the reduction of the support compared with the metal-free $Ce_{0.5}Zr_{0.5}O_2$. A further improvement is observed on sintering induced by repetitive reduction/oxidation processes. Indeed, the temperature of support reduction decreases from 650–950 to about 450 K for the Rh- and Pt-loaded samples and to 520 K in the presence of Pd. In contrast, the low-temperature reduction of Rh/CeO_2 (surface area 194 m^2 g^{-1}) is strongly encumbered after such treatments. The roles of noble metal and added ZrO_2 in promoting low-temperature reduction are discussed.

Key Words: **noble metal; CeO_2–ZrO_2 solid solutions; oxygen storage; temperature-programmed reduction; redox properties; three-way catalyst.**

INTRODUCTION

Traditional three-way automotive catalysts (TWCs) contain platinum-group metals as the active components. Rh is added to the catalyst because its efficiency at NO reduction substantially exceeds that of both Pt and Pd. Rare earth oxides are also incorporated as additives either to improve catalytic performance or to stabilize the catalyst against thermal deactivation. Cerium oxide is widely employed due to its high oxygen storage/release capacity (OSC). The simultaneous conversion of NO, CO, and hydrocarbons in the TWC requires that the air/fuel ratio be close to the stoichiometric value (air/fuel ratio = 14.6). The lambda sensor, installed in vehicles to control the air/fuel ratio, has a certain response time leading to oscillations in the gas composition. CeO_2, acting as a chemical oxygen pressure regulator in the converter, helps the catalyst to cope with the oscillations of the gas stream about the stoichiometric value and allows maintenance of the TWC at high efficiency (1–4).

[1] To whom correspondence should be addressed. Fax: ++39-00-6763903. E-mail: kaspar@univ.trieste.it.

Recently, Pd-only catalysts have been proposed as alternatives to the traditional TWCs. It has been demonstrated that a Pd catalyst promoted by lanthana has activity similar to that of a Rh-containing TWC (5). A major disadvantage of using Pd technology is that high conversion efficiency is obtained in a narrow air-to-fuel (A/F) window. The presence of an efficient "oxygen buffer" is therefore essential. The ability of CeO_2 to act as an oxygen buffer has stimulated strong interest in the investigation of redox properties of CeO_2-based catalysts. However, a major drawback of CeO_2 is that significant deactivation of the redox couple occurs at the high temperatures encountered under typical driving conditions. A great number of systems [e.g., CeO_2–Al_2O_3 (6), CeO_2–SiO_2 (7), CeO_2–La_2O_3 (6), CeO_2–ZrO_2–M_2O_3 (8), CeO_2–HfO_2 (9)] have been examined with the aim of increasing the thermal stability of CeO_2 and preventing decline of OSC. We have shown that incorporation of ZrO_2 into the CeO_2 lattice strongly promotes the reducibility of metal-loaded mixed oxides. We have observed that in the Rh-loaded $Ce_{1-x}Zr_xO_2$ ($x = 0.1$–0.9, surface area $\leq$ 1.5 m^2 g^{-1}), the addition of an increasing amount of ZrO_2 lowers the temperature of the reduction of bulk Ce^{4+}, reaching a minimum of 600 K for the cubic $Rh/Ce_{0.5}Zr_{0.5}O_2$, ca. 500 K lower than the temperature of reduction of bulk Rh/CeO_2 (10). The ability of $Rh/Ce_{0.5}Zr_{0.5}O_2$ to undergo reduction in the bulk at such a low temperature results in the unusually high oxygen exchange capacity of this support. It should be noted, however, that in the previous study highly sintered, low-surface-area samples were investigated, while for catalytic applications, high surface area is desirable. We have therefore extended our investigation to the reduction/oxidation behavior of high-surface-area samples. Investigation of $Ce_{0.5}Zr_{0.5}O_2$ disclosed an unusual improvement of the redox behavior induced by repetitive reduction/oxidation of the solid solution (11). A preliminary note on the redox behavior of Rh-loaded $Ce_{0.5}Zr_{0.5}O_2$ has also been published (12). The present paper discloses the redox properties of Rh-, Pt-, and Pd-loaded $Ce_{0.5}Zr_{0.5}O_2$. Comparison with data obtained on Rh/CeO_2 is included to elucidate the role of ZrO_2. The influence of

0021-9517/99 $30.00

the thermal/redox treatment on H_2 chemisorption is also addressed.

EXPERIMENTAL

$Ce_{0.5}Zr_{0.5}O_2$ solid solution was synthesized by a homogeneous gel route from $Ce(acac)_4$ and $Zr(O–Bu)_4$ precursors (Aldrich) according to a previous report (11). Briefly, the two precursors were refluxed in ethanol for 2 h, followed by evaporation of the solvent; the resulting gel was aged at 363 K for 2 days and finally dried at 393 K. The solid obtained was calcined at 773 K in air for 5 h. CeO_2 was kindly provided by Dr. L. Murrel. Metal impregnation was carried out by the incipient wetness method using aqueous solutions of $RhCl_3 \cdot nH_2O$, H_2PtCl_6, and $PdCl_2$ (in diluted HCl) to obtain a nominal metal loading of 0.5 wt%. The catalysts were dried at 393 K overnight and calcined at 773 K for 5 h. Henceforth, these samples are indicated as fresh ones.

Temperature-programmed reduction (TPR) experiments were carried out in a conventional system equipped with a thermal conductivity detector. To minimize the contribution from adsorbed species to the TPR, all samples were treated in Ar (20 ml min^{-1}) at 900 K for 5 h before the initial TPR experiment. Separate experiments showed that negligible CO_2 evolution could be detected after such treatment. The TPR characterization was performed on 0.05 g of catalyst, under 5% H_2/Ar, with a constant flow rate of 30 ml min^{-1} and from room temperature to 1273 K (heating rate 10 K min^{-1}). H_2 consumption in the TPR experiment was estimated from the integrated peak areas by comparison with those obtained by using CuO as standard. The reproducibility of the method was periodically checked and a standard deviation for the overall H_2 uptake of ± 0.05 mmol g^{-1} was measured. After TPR, the sample was outgased under an Ar flow at 1273 for 30 min and cooled down to 700 K, where oxidation was carried out by a pulse technique at 700 K to ensure full oxidation in the bulk of the solid solution (10). Pulses of O_2 (0.092 ml) were injected into the flow of Ar passing over the sample until the breakthrough point was obtained. Samples obtained from these treatments are hereafter indicated as aged. To investigate the effects of aging on the redox properties of the samples, the TPR/oxidation cycle above described was typically repeated three times.

Full N_2 adsorption isotherms at 77 K and H_2 chemisorption were carried out on a Micromeritics ASAP 2000 analyzer. The samples ($\approx$0.5–1.0 g) were reduced in a flow of H_2 (20 ml min^{-1}) at a heating rate of 10 K min^{-1} up to the selected reduction temperature (350, 473, or 1000 K). After 2 h at this temperature, samples were evacuated at 673 K for 5 h and cooled under vacuum to the adsorption temperature (233 or 308 K). Typically, an equilibration time of 20 min was employed. The adsorbed volumes were determined by extrapolation to zero pressure of the linear part of the adsorption isotherm, and no corrections to eliminate the so-called reversible hydrogen adsorption were employed. A chemisorption stoichiometry of $H : M = 1 : 1$ was assumed.

Raman spectra were measured on a microfocused system (System 1000, Renishaw plc) which uses the same microscope lens to focus the laser beam onto the sample and to collect the scattered radiation to be analyzed. The dispersed radiation was then collected on a charge coupled device (CCD) and the resulting spectrum stored for subsequent analysis. The vibrational spectra were excited with an Ar^+ laser operating at 514.5 nm; a typical collection time was 15 s with a laser power of about 20 mW on the sample.

Micrographs were taken with a conventional scanning electron microscope (Cambridge Inc.). Before the images were taken, the powders were dispersed in water, a drop of the suspension was dropped onto the specimen holder, and, after the water was evaporated, the powder was coated with gold to prevent charging under the electron beam.

Powder X-ray diffraction patterns were collected on a Siemens 700 diffractometer using Ni-filtered Cu$K\alpha$. The peaks in the XRD patterns were fitted by using Pearson VII functions and the parameters obtained were employed to determine the cell parameters. The TREOR90 program, which employs the Visser algorithm, was used to refine the cell parameters.

RESULTS

Temperature-Programmed Reduction/Oxygen Uptake Measurements

The TPR profile of fresh Rh-loaded $Ce_{0.5}Zr_{0.5}O_2$ shown in trace 1 of Fig. 1 features three peaks at 420, 620, and 1000 K. The peak at 420 K is attributed to the reduction of the noble metal precursor (13). A consumption of 0.023 mmol H_2 g^{-1} is measured for the peak, which is lower than the 0.073 mmol g^{-1} expected for the Rh^{3+} reduction to give Rh^0. The difference may be attributed to the presence of well-dispersed Rh_2O_3, reduction of which may occur even at subambient temperatures (13). Partial decomposition of the rhodium oxide in the pretreatment cannot be discounted. H_2 consumption of 0.68 mmol g^{-1} is measured for the peak at 620 K. This value agrees well with that obtained in the TPR of the pure support which shows two peaks at 880 and 1010 K (11). The presence of the supported Rh does not affect the latter peak, while the former peak is shifted down to 620 K. As written below, $Rh/Ce_{0.5}Zr_{0.5}O_2$ has a surface area of 30 m^2 g^{-1} after the thermal pretreatment (Table 2). Therefore, an H_2 consumption of 0.25 mmol g^{-1} can be calculated on application of the linear relationship between the surface area and H_2 consumption found by Perrichon *et al.* (14). Note that this is an upper limit for H_2 consumption since it is assumed that the surface contains only Ce^{4+} sites. Consequently, the peak at 620 K is

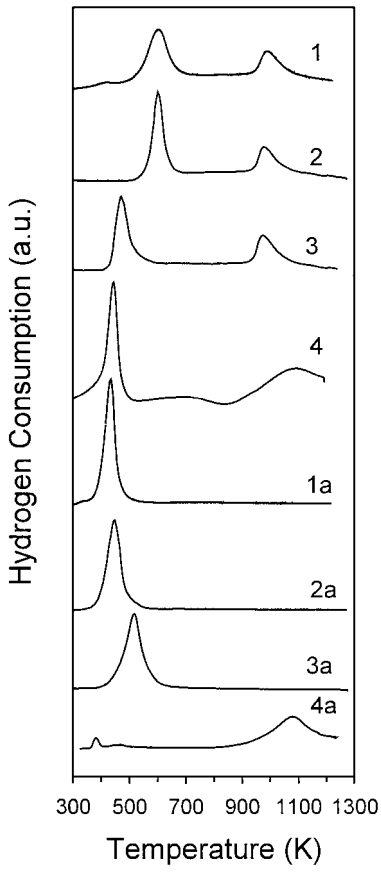

FIG. 1. Temperature-programmed reduction of (1) fresh and (1a) reduced at 1273 K/oxidized at 700 K $Rh/Ce_{0.5}Zr_{0.5}O_2$, (2) fresh and (2a) reduced at 1273 K/oxidized at 700 K $Pt/Ce_{0.5}Zr_{0.5}O_2$, (3) fresh and (3a) reduced at 1273 K/oxidized at 700 K $Pd/Ce_{0.5}Zr_{0.5}O_2$, and (4) fresh and (4a) reduced at 1273 K/oxidized at 700 K Rh/CeO_2.

attributed to reduction occurring both at the surface and in the bulk. After oxidation at 700 K, the sample was again subjected to TPR (Fig. 1, trace 1a). All the reduction features disappear at high temperatures and a single peak at 440 K is observed. In all subsequent reduction/oxidation cycles, the TPR profiles do not change further.

Except for the peak at 420 K, the TPR of the fresh $Pt/Ce_{0.5}Zr_{0.5}O_2$ (Fig. 1, trace 2) is very similar to that of the fresh rhodium-loaded sample. TPR studies of Pt/Al_2O_3 obtained from chlorine-containing precursors have shown that chlorine is strongly retained on the surface. The metal precursor, which can be schematically indicated as $[Pt^{IV}O_xCl_y]$, is reduced at about 600 K. In contrast, the reduction of highly dispersed α-$[PtO_2]$ surface species occurs at about 400 K (15, 16). The relatively mild calcination and pretreatment conditions might not have been able to remove completely the chlorine from the metal precursor. A H_2 consumption of 0.71 mmol g^{-1} has been measured for the peak at 620 K. This value is only slightly higher then that observed for the same peak in the TPR of the Rh loaded sample. A H_2 consumption of 0.05 mmol g^{-1} is expected for the reduction of all Pt^{IV} to Pt^0; 0.20 mmol g^{-1} is the upper limit for H_2 consumption during surface reduction of the support (surface area 18 m^2 g^{-1}, Table 2) (14). These factors indicate that the reduction peak at 620 K is a concomitant reduction of the metal precursor and surface/partially bulk reduction of the support. The peak at 1000 K is associated with further reduction of Ce^{4+} species in the bulk. After oxidation at 700 K, the sample is again subjected to TPR (Fig. 1, trace 2a). A single peak at 450 K is observed. In subsequent reduction/oxidation cycles, the TPR profile shows no changes.

The TPR of fresh $Pd/Ce_{0.5}Zr_{0.5}O_2$ shows two peaks at 470 and 1000 K (Fig. 1, trace 3). No evidence for Pd reduction is found; however, it is well known that the eventual reduction would occur at a subambient temperature. Attribution of the reduction peaks reported in Fig. 1, trace 3, follows that reported above. After oxidation at 700 K, TPR (Fig. 1, trace 3a) shows a single peak at 520 K; this profile is unaffected by subsequent redox cycles.

The comparison with the TPR behavior of Rh/CeO_2 is also shown in Fig. 1. Fresh Rh/CeO_2 (Fig. 1, trace 4) features strong reduction peaks at 440 and 1080 K and a negative peak at about 850 K. The peak at 440 K is associated with the rhodium precursor and CeO_2 surface reduction. The latter process is promoted by the supported metal. The peak at 1080 K is associated with the reduction of CeO_2 in the bulk (3, 4). Negative peaks have previously been observed and attributed to desorption of H_2 and/or evolution of carbonates from the bulk of the support (17). After oxidation at 700 K, TPR showed only two minor peaks below 500 K, which can be attributed to the reduction of Rh_2O_3 of different particle sizes (10). The contribution of the support to the reduction at low temperatures is lost and the peak at 1080 K is the only relevant reduction feature remaining (Fig. 1, trace 4a).

O_2 uptakes measured in the oxidation experiments are summarized in Table 1. H_2 consumption is also included. As shown by Zotin *et al.* (18), the accuracy of the measurements of the degree of reduction should, from the TPR profiles of CeO_2-based catalysts, be poor, due to a number of concomitant phenomena that affect the profiles (reduction/desorption of surface/bulk impurities). Under our experimental conditions such phenomena should be minimized; however, H_2 adsorption/desorption phenomena (19, 20) could well be present. In fact, overall H_2 consumption exceeds to some extent the corresponding O_2 uptake in the $NM/Ce_{0.5}Zr_{0.5}O_2$ catalysts. In particular, fresh $NM/Ce_{0.5}Zr_{0.5}O_2$ shows overall H_2 consumption about 20% higher than the corresponding O_2 uptake. This excess is decreased by redox cycling. Good agreement between the two pieces of data is observed for the CeO_2-based systems.

At 700 K H_2 is desorbed (19, 21) and the degree of support reduction can be related to the formation of oxygen

TABLE 1

H_2 Consumption and O_2 Uptake Measured in the TPR/Oxidation Experiments Carried Out on Metal-Free and Metal-Loaded $Ce_{0.5}Zr_{0.5}O_2$ and CeO_2

Sample	Number of recycles	Peak temperature (K)	H_2 consumption (mmol g^{-1})	O_2 uptake[a] (mmol g^{-1})	x in $Ce_mZr_{1-m}O_x$[b] ($m = 0.5, 1$)	Ce^{3+}[b] (%)
$Ce_{0.5}Zr_{0.5}O_2$	0	880, 1010	0.71, 0.40	0.53	1.845	63
	2–7	664–675, 745–756, 839–858	0.13–0.36, 0.62–0.71, 0.22–0.31	0.46	1.865	55
	8[c]		1.03	0.44	1.870	52
$Rh/Ce_{0.5}Zr_{0.5}O_2$	0	420, 620, 1000	0.023, 0.68, 0.55	0.49	1.855	58
	1–3	440	1.12	0.53	1.845	63
	4[d]			0.43	1.875	50
$Pt/Ce_{0.5}Zr_{0.5}O_2$	0	620, 1000	0.72, 0.52	0.52	1.845	61
	1–3	450	1.12	0.50	1.85	59
	4[d]			0.45	1.865	54
$Pd/Ce_{0.5}Zr_{0.5}O_2$	0	470, 1000	0.71, 0.51	0.53	1.845	62
	1–3	520	1.12	0.50	1.85	59
	4[d]			0.30	1.91	35
	5[e]			0.46	1.86	54
CeO_2	0	790, 1100	0.42, 0.57	0.50	1.83	35
	1–3	1100	0.89	0.50	1.83	35
	4[c]			0.02	1.99	2
Rh/CeO_2	0	440, 1080	0.57, 0.64	0.59	1.80	41
	1	380, 460, 1075	1.02	0.58	1.81	40
	2[c]			0.02	1.99	2

[a] Measured after the TPR experiment carried out up to 1273 K; SD, ±0.01 mmol g^{-1}.
[b] Estimated from O_2 uptake at 700 K, values not corrected for metal oxidation.
[c] Isothermal reduction at 600 K for 2 h.
[d] Isothermal reduction at 440 K for 2 h.
[e] Isothermal reduction at 500 K for 2 h.

vacancies in the solid solution due to the reducible Ce^{4+} cation,

$$2CeO_2 \rightarrow 2Ce^{I}_{Ce} + V_0^{\bullet\bullet} + \tfrac{1}{2}O_2 + 3O^x_o,$$

where, according to Kröger–Vink notation, Ce^{I}_{Ce}, $V_o^{\bullet\bullet}$, and O^x_o represent, with respect to the lattice sites, the negatively charged Ce^{3+}, the double positively charged oxygen vacancy, and a neutral oxygen site. For CeO_2, single ionized oxygen vacancies were reported only for large deviations from stoichiometry (22). The degree of reduction is therefore best evaluated from O_2 uptake (10, 18). Even if some reduction of surface Zr^{4+} cannot be excluded, attribution of the redox processes essentially to the Ce^{3+}/Ce^{4+} redox couple appears highly reasonable. Indeed, Borer *et al.* (23) found only a minor Zr^{4+} reduction for a Rh-loaded zirconia dispersed on SiO_2 below 1200 K. The degree of reduction is therefore reported in Table 1 both as percent of Ce^{3+} or as x in $Ce_mZr_{1-m}O_x$ ($m = 0.5$, 1 is the Ce molar fraction), where $2 - x$ represents the total amount of oxygen vacancies formed by reduction of the solid. At 700 K a partial metal oxidation certainly occurs (24). Keeping in mind the low metal loading and the uncertainty on the final oxidation state (15), the degree of reduction is reported without subtraction of the contribution due to the metal oxidation.

Modification of the Texture, Structural Properties, and Surface Area Induced by the Redox Cycles:

N_2 physisorption at 77 K. The influence of the thermal treatments on textural properties was investigated by means of N_2 physisorption at 77 K (Table 2). All samples show isotherms of type IV and H2 hysteresis according to the IUPAC classification which are indicative of the presence of a mesoporous texture (25). The isotherm of fresh Rh/CeO_2 reveals a substantial contribution from micropores (BET constant $c = 112$). From the adsorbed volume-versus-t plot, a microporous area of 34 m^2 g^{-1} is calculated according to Harkins and Jura (26). In the case of fresh $Rh/Ce_{0.5}Zr_{0.5}O_2$, the contribution of the micropores to the surface area is minimal and is completely absent in the Pt- and Pd-loaded samples (Table 2). Impregnation of $Ce_{0.5}Zr_{0.5}O_2$ with the noble metal solution and subsequent calcination induce a decrease in surface area, even if the total pore volume is almost unaffected. The degree of sintering is a function of the nature of the metal and increases in the order Rh < Pt < Pd.

TABLE 2

Textural Characterization of Metal-Free and NM-Loaded CeO_2 and $Ce_{0.5}Zr_{0.5}O_2$ and Effects of Modifications Induced by *in Situ* Thermal and H_2 Treatments[a]

Sample	Treatment[b]			BET area ($m^2\ g^{-1}$)	Pore volume ($ml\ g^{-1}$)[c]			
					Total	Mesopore	Micropore	
	T (K)	Gas	Time (h)			V_{BJH}	V_t	V_{DR}
$Ce_{0.5}Zr_{0.5}O_2$	—	—	—	64	0.06	0.04	0.03	0.025
	1000	H_2	2	12	0.06	0.06	—	—
$Rh/Ce_{0.5}Zr_{0.5}O_2$	—	—	—	53	0.07	0.06	0.01	0.02
	900	N_2	5	30				
	473	H_2	2	29				
	1000	H_2	2	18	0.05	0.05	—	0.005
$Pt/Ce_{0.5}Zr_{0.5}O_2$	—	—	—	42	0.05	0.05	—	—
	900	N_2	5	18			—	—
	473	H_2	2	18			—	—
	1000	H_2	2	10	0.05	0.05	—	—
$Pd/Ce_{0.5}Zr_{0.5}O_2$	—	—	—	35	0.05	0.05	—	—
	900	N_2	5	11			—	—
	473	H_2	2	11			—	—
	1000	H_2	2	11	0.05	0.05	—	—
CeO_2	—	—	—	196	0.15	0.08	0.08	0.08
	1000	H_2	2	12	0.04	0.04	—	—
Rh/CeO_2	—	—	—	194	0.17	0.09	0.06	0.08
	900	N_2	5	164				
	473	H_2	2	154				
	1000	H_2	2	38	0.09	0.085	—	0.01

[a] All the samples were evacuated at 623 K to a constant pressure $\leq 2 \times 10^{-3}$ Torr prior to N_2 adsorption.

[b] Treatment in flow of N_2 (20 ml min^{-1}), H_2 (20 ml min^{-1}); before N_2 adsorption, the reduced samples were oxidized at 700 K.

[c] Values determined from the adsorption isotherm by using the BHJ method in the range 3.5–170 nm and the t plot and the Dubinin–Radushkevich plot in the range 2×10^{-5} to $0.1p/p_0$. Total pore volume calculated at $p/p_0 = 0.98$ according to Gurvitsch rule.

On thermal treatment at 900 K, all samples show a significant decrease in surface area, which in the case of Rh/CeO_2 is associated mainly with a loss of microporosity (14). Remarkably, in the presence of Pd, this treatment induces full collapse of the surface area (11 $m^2\ g^{-1}$) and no appreciable modification of the texture is observed on further H_2/O_2 treatments. Further reduction at 473 K, e.g., at surface reduction temperature, does not significantly decrease the surface area of the samples. A significant loss of surface area is observed after reduction at 1000 K, e.g., at a bulk reduction temperature. Notably, the supported Rh interferes with the sintering of the support (Table 2). The supported Rh clearly hinders the collapse of surface area since for both CeO_2 and $Ce_{0.5}Zr_{0.5}O_2$ an area of 12 $m^2\ g^{-1}$ was observed after reduction at 1000 K. The redox cycles destroy all the microporosity initially present while no significant decrease in pore volume due to mesopores is observed. The N_2 isotherms of the recycled samples are still type IV, but the hysteresis changes to type H3. This is an indication of extensive pore restructuring. We calculate, according to Barret, Joyner, and Halenda (BJH) (27), average pore diameters of 6.5 and 15–19 nm for Rh/CeO_2 and $NM/Ce_{0.5}Zr_{0.5}O_2$ respectively. In contrast, the fresh samples show a porosity only below 5 nm.

Raman spectra of the fresh and recycled samples. The modification of the structural properties of $NM/Ce_{0.5}Zr_{0.5}O_2$ on redox cycles was investigated by Raman spectroscopy. The Raman spectra of fresh and recycled $NM/Ce_{0.5}Zr_{0.5}O_2$ are shown in Fig. 2. The spectra of fresh $NM/Ce_{0.5}Zr_{0.5}O_2$ are characterized by three bands: a very broad band at about 620 cm^{-1}, a strong band centered at 465 cm^{-1}, and a very weak band at 313 cm^{-1}. The observed Raman patterns suggest an attribution of fresh samples to a t'' phase according to the classification proposed by Yashima *et al.* (28). These spectra are similar to that of unsupported $Ce_{0.5}Zr_{0.5}O_2$, with the exception of the band at 620 cm^{-1}, the intensity of which is increased in the presence of the supported noble metal. This increase in intensity could be tentatively associated with some oxygen vacancies due to partial incorporation of oxidized NM species in the support (29). A high-frequency tail to the Raman mode at 465 cm^{-1} was observed in CeO_2–trivalent rare earth mixed oxides and was associated with the oxygen

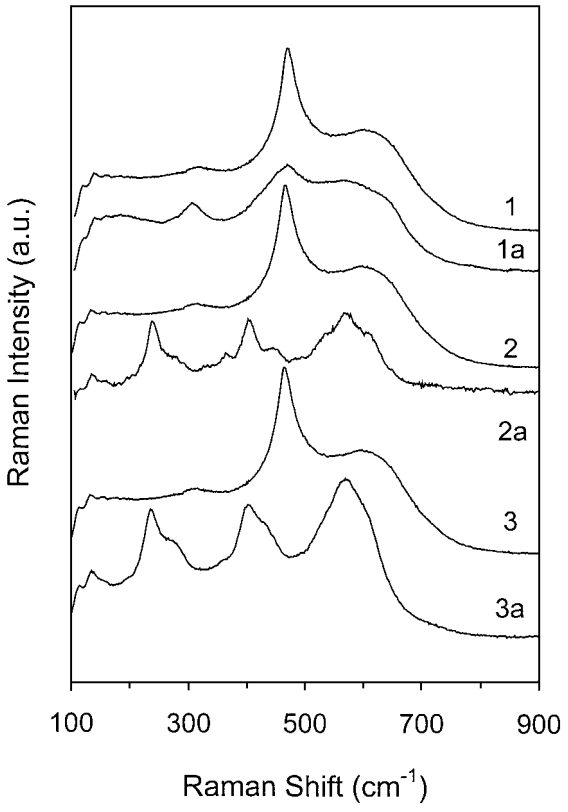

FIG. 2. Raman spectra of (1) fresh and (1a) reduced at 1273 K/oxidized at 700 K $Rh/Ce_{0.5}Zr_{0.5}O_2$, (2) fresh and (2a) reduced at 1273 K/oxidized at 700 K $Pt/Ce_{0.5}Zr_{0.5}O_2$, and (3) fresh and (3a) reduced at 1273 K/oxidized at 700 K $Pd/Ce_{0.5}Zr_{0.5}O_2$.

vacancies created on Ce^{4+} substitution (30). By redox cycling the $NM/Ce_{0.5}Zr_{0.5}O_2$ samples, the Raman spectra are strongly modified: the intensity of the peak at 465 cm^{-1} strongly decreases (Rh sample) or it disappears (Pt and Pd samples). In $Pt/Ce_{0.5}Zr_{0.5}O_2$ Pt and $Pd/Ce_{0.5}Zr_{0.5}O_2$ (Fig. 2 traces 2a and 3a) six bands are observed respectively at 606–602, 573–570, 447–430, 403–402, 275–270, and 236–235 cm^{-1} which are consistent with a tetragonal symmetry (28). The small shift in the positions of the bands is probably due to small change in the stoichiometry of the Pd and Pt samples.

XRD and SEM Characterization

The powder X-ray patterns of the fresh and reduced/oxidized $NM/Ce_{0.5}Zr_{0.5}O_2$ samples are reported in Fig. 3. The fresh samples show rather broad peaks attributed to the presence of small crystallites which are formed after calcination at 773 K. An estimate of the average particle size of $Ce_{0.5}Zr_{0.5}O_2$ by the line broadening method gives a value of around 5 nm for all the fresh samples (Table 3). The width of the XRD peaks does not allow an unequivocal assignment of the reported pattern. In fact the tetragonal t' phase is usually distinct from the cubic one on the base of the splitting of the peaks observed in CeO_2 at about 47° and 49° (2θ). The XRD peaks of fresh $NM/Ce_{0.5}Zr_{0.5}O_2$ are slightly asymmetric. This is due to the presence of a residual amount (<8%) of an almost pure CeO_2 phase, as observed in the pure support (11).

After reduction at 1273 K and oxidation at 700 K, the width of all the XRD peaks strongly decreases, indicating extensive sintering. The average particle diameter of the recycled Rh-loaded sample is about twice that of the fresh sample. In the case of Pt and Pd the increase in particle diameter induced by the redox treatments is much stronger (Table 3). The main peaks of the XRD patterns are indexed in a $Fm3m$ space group, indicating that the cubic symmetry of the cation sublattice is retained on redox treatment.

No diffraction peak due to the presence of Rh and Pt is observed in the samples (Fig. 3 traces 1 and 2a). Two very weak diffraction features, which might be associated with the presence of Pd, appear in the XRD diffraction pattern of $Pd/Ce_{0.5}Zr_{0.5}O_2$, as reported in Fig. 3, traces 3 and 3a.

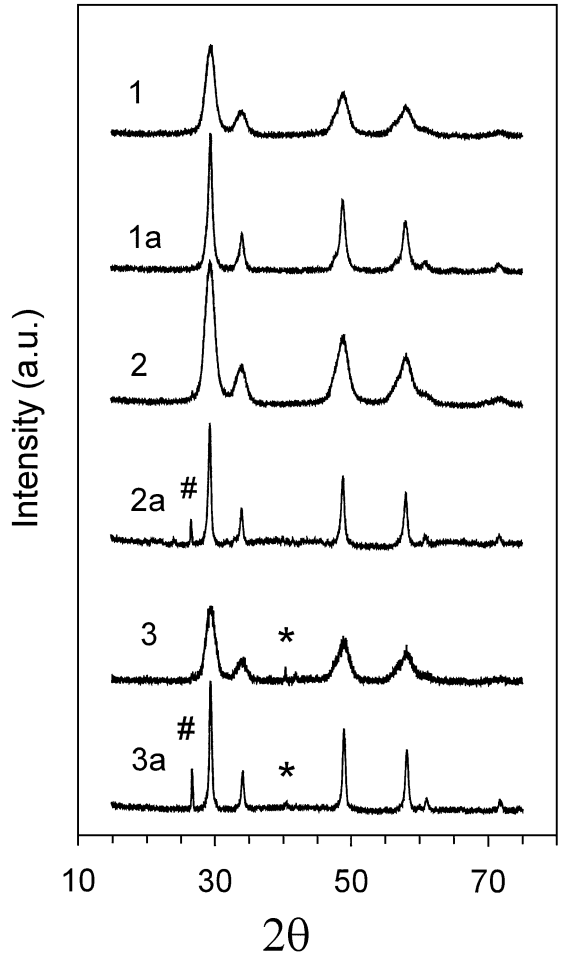

FIG. 3. XRD patterns of (1) fresh and (1a) reduced at 1273 K/oxidized at 700 K $Rh/Ce_{0.5}Zr_{0.5}O_2$, (2) fresh and (2a) reduced at 1273 K/oxidized at 700 K $Pt/Ce_{0.5}Zr_{0.5}O_2$, and (3) fresh and (3a) reduced at 1273 K/oxidized at 700 K $Pd/Ce_{0.5}Zr_{0.5}O_2$. #, quartz; ∗, Pd/PdO (see text).

TABLE 3

Powder XRD Characterization of NM/$Ce_{0.5}Zr_{0.5}O_2$

Catalyst		Cell parameter *a* (Å)	Particle size (nm)
$Rh/Ce_{0.5}Zr_{0.5}O_2$	Fresh	5.270	5.4
	Recycled	5.267	12.7
$Pt/Ce_{0.5}Zr_{0.5}O_2$	Fresh	5.271	5.0
	Recycled	5.267	22.0
$Pd/Ce_{0.5}Zr_{0.5}O_2$	Fresh	5.271	5.1
	Recycled	5.260	27.8
$Ce_{0.5}Zr_{0.5}O_2$ [a]	Fresh	5.265	5.4
	Recycled		68

[a] Data from Ref. (11).

The broad features at 40.4° and 41.9° could correspond to the (111) Pd and (110) PdO peaks, respectively (31). The other peaks characteristic of Pd or PdO are not observed, but their relative intensities are much lower compared with those of the above-mentioned peaks. It should be recalled that in all cases the metal loading is small (0.5%) and therefore any metal determination from XRD is difficult, especially when the metal is well dispersed on the support surface.

Scanning election micrographs of three fresh and recycled samples are reported in Fig. 4. The most striking feature is exhibited by the Rh-loaded sample, since it is barely possible to detect any difference before and after the recycling treatment. Conversely, the Pt-loaded sample seems to undergo extensive coarsening and sintering, with a morphology typical of liquid phase-assisted sintering. Somewhat intermediate is the behavior of the Pd-loaded sample: some microstructural rearrangement occurs, as demonstrated by the rounding of the particles in the recycled sample and the disappearance of the sharp edges and corners originally present in the fresh sample. The scale of the rearrangement, however, seems to remain limited to a size of about 50–100 μm, whereas the mesoscopic scale remains unaffected.

In summary, the scanning electron micrographs of the fresh and recycled samples indicate a significant difference between the Rh sample on one side and the Pd and Pt samples on the other. As can be seen in the micrographs the latter two exhibit extensive coarsening and sintering, whereas Rh remains less affected on the scale under observation.

Volumetric Hydrogen Adsorption

Table 4 summarizes the results of volumetric hydrogen studies of chemisorption on Rh-, Pt-, and Pd-loaded $Ce_{0.5}Zr_{0.5}O_2$ and Rh/CeO_2. In view of the above TPR results, the catalysts were reduced at low and high temperatures (350, 473, and 1000 K). The estimation of the metal particle size from H_2 adsorption on Rh/CeO_2 catalysts is difficult due to its extensive adsorption on the support (32, 33). However, the amount of H_2 spilled over the support can be minimized by lowering the H_2 adsorption temperature. This allows determination of H_2 chemisorbed on the Rh particles (32, 33). The apparent H/Rh ratios were therefore measured at 233 and 308 K. The same procedure has been adopted for measuring Pt dispersion. In the case of Pd, H_2 chemisorption at low temperature could not be used due to the formation of Pd β-hydride which does not allow the exact chemisorption stoichiometry to be calculated (34). Accordingly, palladium dispersion has been measured at 308 K in the low-pressure region of the adsorption isotherm (1–4 Torr). It is worth noting that the use of low H_2 pressure intrinsically hinders extensive H_2 adsorption on the support. Further, it has been shown that prolonged thermal/evacuation treatment and use of room-temperature low-H_2-pressure chemisorption allow determination of the metal dispersion in $Pd/Ce_{0.6}Zr_{0.4}O_2/Al_2O_3$ (35).

The H/Rh = 0.86 value measured at 308 K over $Rh/Ce_{0.5}Zr_{0.5}O_2$ is about three times that determined at 233 K, suggesting a significant contribution from H_2 spillover. After evacuation at 673 K, the H/Rh measured at 308 K is still twice that measured at 233 K, while equal values are measured after treatment at 900 K in N_2. Note that H/Rh = 0.27 was obtained at 233 K in these experiments, which indicates that, despite the strong textural variation of $Ce_{0.5}Zr_{0.5}O_2$, no measurable variation of exposed surface metal area has occurred. The equal H/Rh ratios measured at 233 and 308 K after treatment at 900 K indicate that we cannot detect any significant amount of H_2 being spilled over the support

TABLE 4

Hydrogen Chemisorption on NM/$Ce_{0.5}Zr_{0.5}O_2$ (NM = Rh, Pt, Pd) and Rh/CeO_2

Catalyst	Reduction temperature (K)	H/NM[a] (308 K)	H/NM[a] (233 K)
$Rh/Ce_{0.5}Zr_{0.5}O_2$	473[b]	0.86	0.27
	473[c]	0.53	0.27
	473[d]	0.27	0.27
	1000	0.21	0.20
	350[e]	1.36	0.44
$Pt/Ce_{0.5}Zr_{0.5}O_2$	473[d]	0.69	0.22
	1000	0.11	0.10
	350[e]	0.18	0.10
$Pd/Ce_{0.5}Zr_{0.5}O_2$	350[d]	0.64	—
	473[d]	0.03	—
	1000	0.01	—
	350[a]	0.05	—
Rh/CeO_2	473[d]	0.80	0.21
	1000	0.14	0.15

[a] Hydrogen chemisorption measured at the indicated temperature.
[b] Fresh sample.
[c] Sample degassed *in vacuo* at 673 K for 5 h before reduction.
[d] Sample pretreated in N_2 at 900 K for 5 h before reduction.
[e] Sample reduced at 1000 K and oxidized at 700 K before reduction.

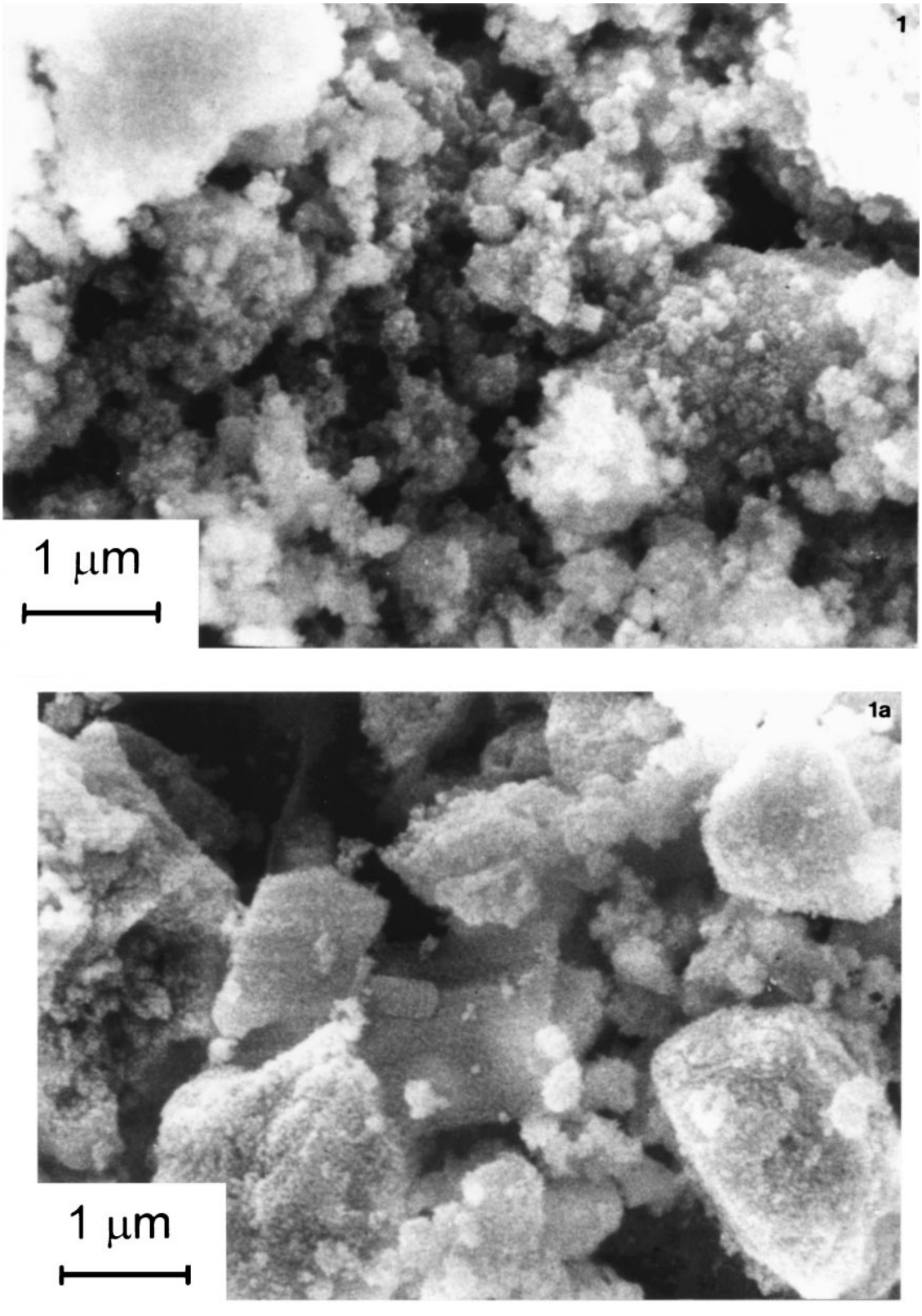

FIG. 4. Scanning electron micrographs of (1) fresh and (1a) reduced at 1273 K/oxidized at 700 K Rh/$Ce_{0.5}Zr_{0.5}O_2$, (2) fresh and (2a) reduced at 1273 K/oxidized at 700 K Pt/$Ce_{0.5}Zr_{0.5}O_2$, and (3) fresh and (3a) reduced at 1273 K/oxidized at 700 K Pd/$Ce_{0.5}Zr_{0.5}O_2$.

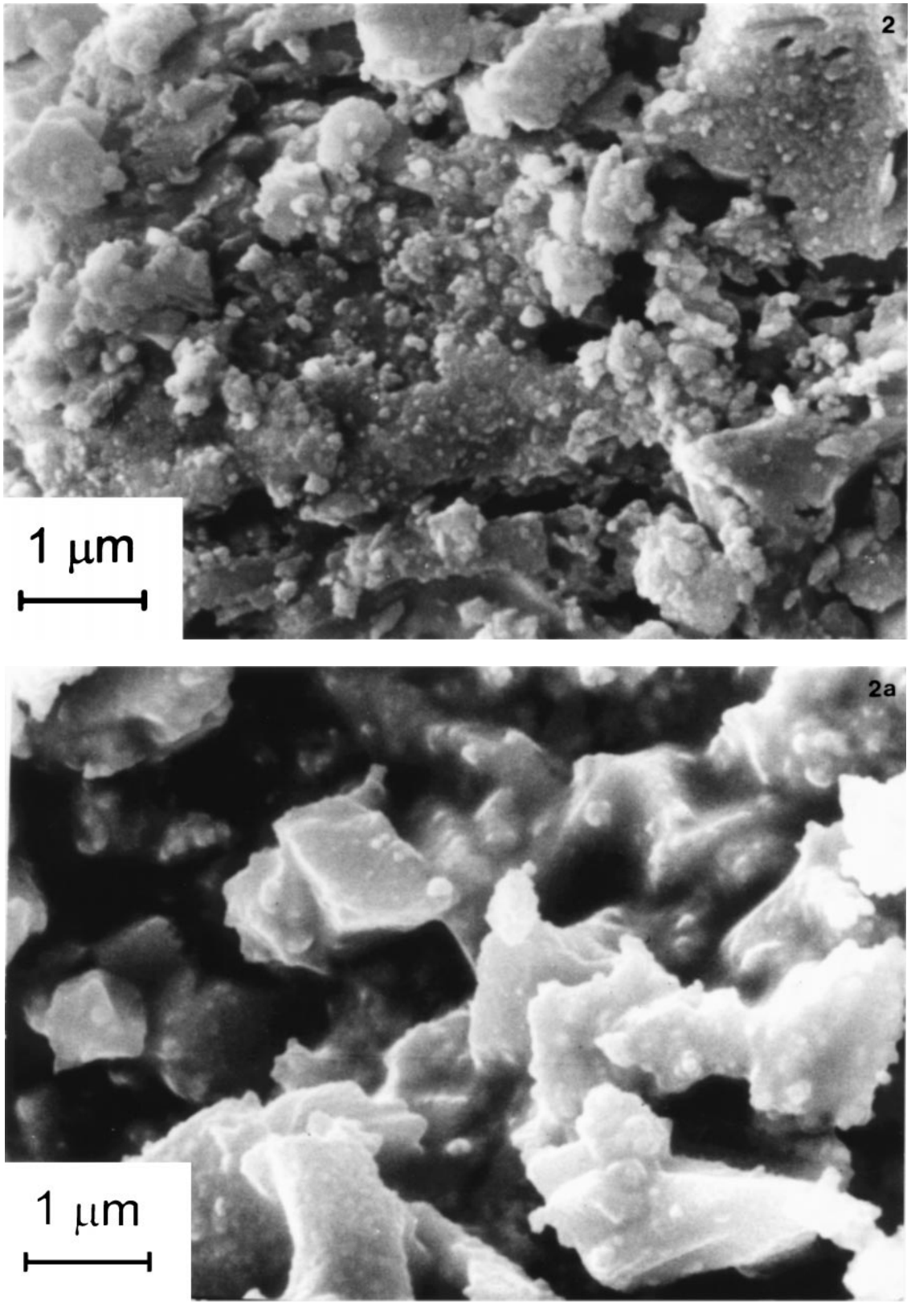

FIG. 4—*Continued*

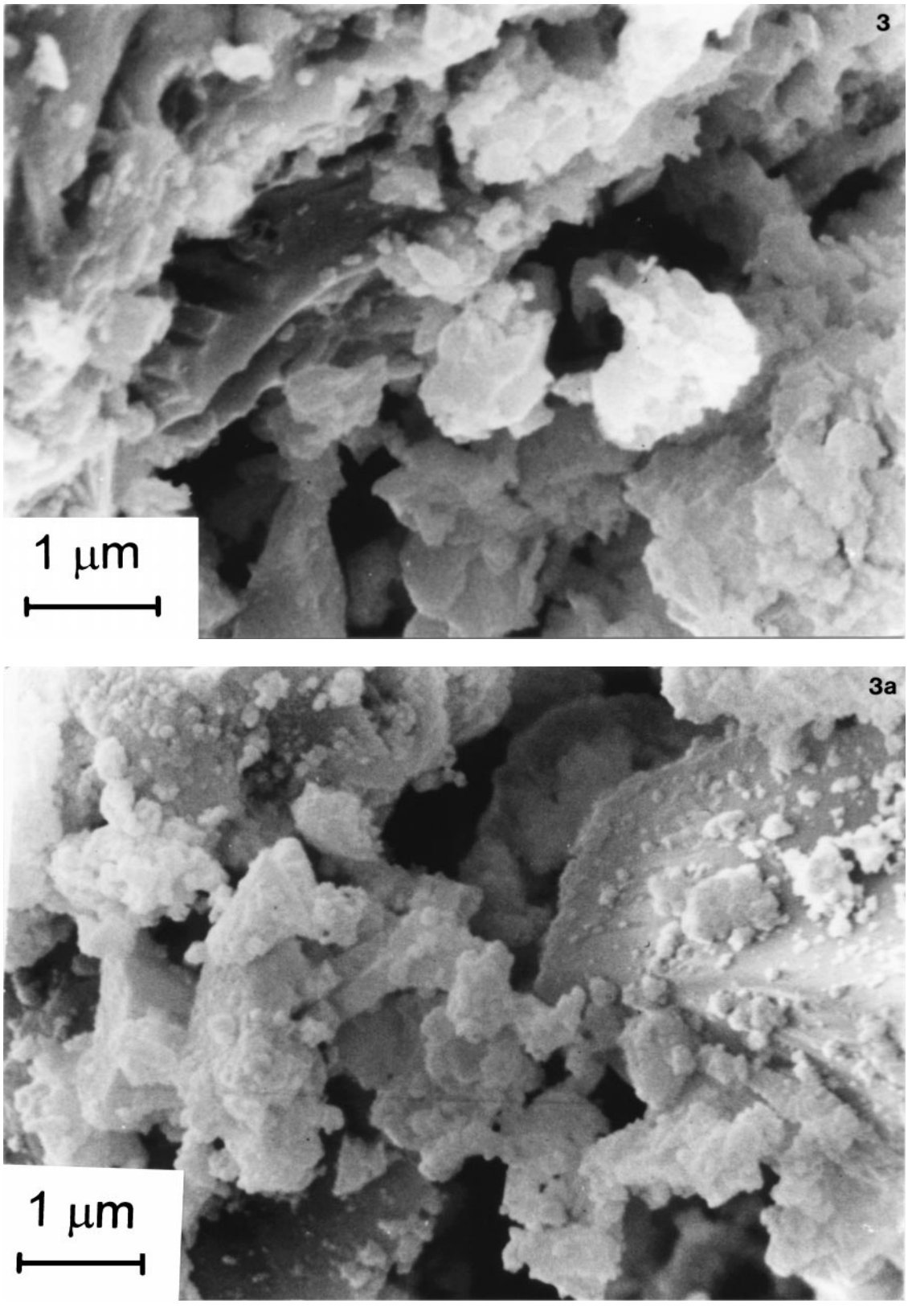

FIG. 4—*Continued*

under the present experimental conditions. In contrast, the H/Rh ratios in Rh/CeO_2 change with adsorption temperature after treatment at 900 K (Table 4). After the reduction at 1000 K, no evidence for H_2 spillover is found in both $Rh/Ce_{0.5}Zr_{0.5}O_2$ and Rh/CeO_2. In the light of the results of the TPR, the sample was oxidized in a flow of oxygen at 700 K and then reduced at 350 K before the H_2 chemisorption measurement. Note that the reduction temperatures were chosen to determine the total capacity of the metal to activate H_2 by keeping reduction of the support to the minimum. Therefore, the reduction was carried out at 473 K for fresh $Rh/Ce_{0.5}Zr_{0.5}O_2$ and 350 K for the recycled sample. Table 4 shows a very high value for H/Rh measured at 308 K over recycled $Rh/Ce_{0.5}Zr_{0.5}O_2$. This value is higher than that observed on fresh catalyst and it is three times that determined at 233 K. The H/Rh measured at 233 K over the recycled sample is higher than that determined at the same temperature for the sample reduced at 473 and that reduced at 1000 K. Even if metal redispersion cannot be excluded, the high efficiency of H_2 spillover at 308 K measured over the recycled sample suggests some residual contribution of H_2 spillover at 233 K.

After treatment at 900 K, the H/Pt ratios vary with adsorption temperature in $Pt/Ce_{0.5}Zr_{0.5}O_2$, while no variation of H/Pt with adsorption temperature is observed after reduction at 1000 K (Table 4). Note that H/Pt is half after the latter treatment. The effects of reduction/oxidation appear similar to $Rh/Ce_{0.5}Zr_{0.5}O_2$ but the extent of restoration of H_2 spillover is limited.

The H/Pd value measured at 308 K over $Pd/Ce_{0.5}Zr_{0.5}O_2$ reduced at 350 K is close to that observed for the Pt-loaded sample, where significant H_2 spillover occurred. That may suggest the N_2 pretreatment at 900 K is able to suppress H_2 spillover to a large extent only in the case of $Rh/Ce_{0.5}Zr_{0.5}O_2$. A low reduction temperature has been chosen accordingly with the ease of reduction of palladium oxide. Noteworthy is that a higher reduction temperature, which also involves reduction in the bulk of the support (i.e., 473 or 1000 K, compare TPR), induces collapse of the hydrogen adsorption capacity of the system. At variance with Rh- and Pt-loaded samples, after oxidation only a minor increase in H/Pd has been observed.

DISCUSSION

The present results disclose an important role of supported Pt, Pd, and Rh in improving the redox properties of $Ce_{0.5}Zr_{0.5}O_2$ at low temperatures. A satisfactory understanding of the redox properties of the investigated samples must consider the following cooperative effects: the relative stability of the noble metal surface, its efficiency in H_2 activation and spillover, and the promotion of Ce^{4+} reducibility due to structural changes of the support induced by redox treatments.

Redox Behavior and H_2 Chemisorption

Let us first consider the general aspects of the TPR profiles. All the fresh $NM/Ce_{0.5}Zr_{0.5}O_2$ features two major reduction peaks respectively at 400–600 and 1000 K. The position of the latter peak is almost independent of the nature of the noble metal, and it disappears on redox cycling. The position of the former peaks depends on the nature of the noble metal, and except for Pd, this peak shifts to a lower temperature on redox cycling.

The disappearance of the peak at 1000 K and improvement of reduction at low temperatures are consistent with the effects of redox cycling on the unsupported sample (11). XRD spectra show that the cation sublattice preserves the cubic *Fm*3*m* symmetry while the strong modification of the relative intensity of the Raman bands in the recycled samples indicates a distortion in the oxygen sublattice. This is consistent with the idea that the improvement in reduction at low temperatures is due to increased displacement of oxygen anions from the tetrahedral sites induced by thermal sintering of the $Ce_{0.5}Zr_{0.5}O_2$ under reducing conditions (11). The oxygen displacement favors high oxygen mobility in the bulk, accounting for the modification of the redox behavior of CeO_2–ZrO_2 mixed oxides. Consistently, EXAFS characterization of low-surface-area $Rh/Ce_{0.5}Zr_{0.5}O_2$ disclosed that the insertion of ZrO_2 into the CeO_2 modifies the oxygen sublattice (36). Some of the oxygens coordinated to the Zr^{4+} preserve the typical Zr–O distances, while two oxygens are pushed away from the Zr to a nonbonding distance longer than 0.28 nm, suggesting a high lability. Removal of two oxygens per Zr atom leads to a final stoichiometry of $Rh/Ce_{0.5}Zr_{0.5}O_{1.75}$. In fact, fewer oxygen vacancies are created in the reduction at 1273 K of $Rh/Ce_{0.5}Zr_{0.5}O_2$ (Table 1), suggesting that formation of a nonstoichiometric defective compound might limit the total degree of reduction. In Rh/CeO_2, no distortion of the oxygen sublattice is observed, hence reduction in the sintered sample occurs at high temperature.

Attribution of the reduction feature at 1000 K to sample nonhomogeneity cannot, however, be discounted. In fact, it appears that crystallographically pure CeO_2–ZrO_2 phases mainly present a single reduction feature (8). On recycling, the XRD peaks appear symmetric, suggesting that the CeO_2 impurity might have been incorporated into a solid solution. The presence of a single reduction feature is consistent with recent computer simulation results, which indicates surface and bulk reduction occurring at comparable temperatures (37).

The variation of the position of the peak at 400–600 K is intriguing and it seems to be attributed to a number of causes, related to the specific nature of the noble metal. For $Rh/Ce_{0.5}Zr_{0.5}O_2$, we observe that the initial treatment at 900 K mainly depresses H_2 spillover, besides causing some loss of surface area. The presence of a spillover killer, such as chlorine (32), not eliminated from the metal precursor

during the calcination and thermal pretreatment, may play an important role in blocking spillover. Despite the low H_2 spillover capacity of pretreated $Rh/Ce_{0.5}Zr_{0.5}O_2$, the noble metal significantly favors the support reduction. The first reduction peak of the bare $Ce_{0.5}Zr_{0.5}O_2$ is shifted down to 620 K in the presence of Rh. In Rh/CeO_2, where the H_2 spillover efficiency after thermal pretreatment is higher, this peak is shifted down to 440 K, suggesting that the higher the spillover rate, the lower the reduction temperature. The presence of ZrO_2 seems to be responsible for the easier suppression of spillover in $Rh/Ce_{0.5}Zr_{0.5}O_2$ compared with Rh/CeO_2. However, it should be also noted that the surface area of fresh CeO_2 is three times than that of fresh $Ce_{0.5}Zr_{0.5}O_2$. It is well known that the higher the CeO_2 surface area, the easier is the surface reduction. After treatment at 900 K, there is a 45% drop in surface area in the case of $Rh/Ce_{0.5}Zr_{0.5}O_2$, while the surface area of Rh/CeO_2 decreases only by 15% (Table 2). Therefore, the less significant shift in the reduction temperature of $Rh/Ce_{0.5}Zr_{0.5}O_2$ compared with Rh/CeO_2 could also be related to the surface area of the support and its stability.

The high-temperature reduction reached during TPR would easily lead to encapsulation of some of the metal particles, even if a simple sintering of Rh particles cannot be excluded. In fact, a decrease of the H/Rh ratio from 0.27 to 0.20 has been observed after reduction at respectively 473 and 1000 K. This should make reduction at low temperatures unfavorable in the subsequent TPR. The opposite is noted: after oxidation at 700 K [oxidation of both the support and Rh particles occurs under these conditions (24)], the peak at 620 K is shifted to 440 K in the TPR profile of recycled $Rh/Ce_{0.5}Zr_{0.5}O_2$. In agreement that an efficient H_2 activation and its spilling over the support are important factors in the reduction process, we note a recovery of the H_2 spillover in the H_2 chemisorption.

Contribution of a SMSI effect to the present chemisorption behavior cannot be excluded. In fact, covering of the metal by the support/metal decoration (SMSI phenomenon) has been proposed to account for the strong inhibition of CO adsorption on Rh/CeO_2 (38). Moreover, recent high-resolution electron microscopy results showed that there are two steps to the microstructural evolution of low-surface-area Rh/CeO_2 on reduction: (i) up to 773 K, growth of Rh particles; (ii) above 973 K, rhodium decoration by ceria (39). It should, however, be noted that except for the Pd-loaded sample, there is a relatively small decrease in H_2 chemisorption after reduction at 1000 K. Further, the variation of H_2 chemisorption with adsorption temperature indicates that H_2 spillover plays a key role in the chemisorption results obtained rather than a blocking of the metal adsorption sites by the support.

Although the Pt- and Rh-loaded samples show very similar TPR profiles, the role of the noble metal and of the support on the redox properties is different. In $Pt/Ce_{0.5}Zr_{0.5}O_2$, thermal treatment does not block H_2 spillover but probably only decreases its extent. Reduction of the metal precursor occurs above 550 K which is associated with the presence of residual chlorine (15, 16). The chemisorption results show that platinum oxychlorine reduction also occurs at 473 K, but it should be noted that in this case pure H_2 has been used for 2 h. As soon as Pt metal is present, H_2 is efficiently activated and it spills over the support, inducing a concomitant reduction of Ce^{4+}. The H_2 spillover capacity of the pretreated $Pt/Ce_{0.5}Zr_{0.5}O_2$ is higher than that of $Rh/Ce_{0.5}Zr_{0.5}O_2$ but the surface area is lower. The combined effect of these properties leads to a support reduction at the same temperature for the two systems. After high-temperature reduction, the H/Pt ratio is half that after low-temperature reduction, suggesting that both sintering and encapsulation of the metal particles could occur. In contrast to the Rh-loaded sample, the sintering effects are more important, as is also confirmed by SEM and XRD. After reduction at 1273 K and oxidation at 700 K, H_2 spillover is partially restored. Removal of residual chlorine (chlorine lowers the reduction of platinum oxide) and the deep structural change to the support, which indicates a transition of M–O bond symmetry from cubic to tetragonal, both favor a decrease in reduction temperature of the support.

Finally, the fresh Pd-loaded sample shows the best redox properties due to the well-known high efficiency of Pd in H_2 activation at low temperature. Reduction at 350 K gives a high H/Pd ratio, while reduction at higher temperature induces a collapse of the H/Pd ratio. A recent investigation on the metal–support interaction in Pd/CeO_2 has shown that the variation in the palladium-exposed area is related to surface area stability (40). Well-dispersed Pd on high-surface-area ceria is irreversibly encapsulated into ceria at reduction temperatures higher than 623 K, while Pd particles supported on low-surface-area ceria are simply decorated by reduced ceria. This decoration was partially reversible on oxidation at high temperature (873 K) (40). Other evidence for encapsulation of Pd by $Ce_{0.5}Zr_{0.5}O_2$ has recently been reported (31). We note that the surface area of $Pd/Ce_{0.5}Zr_{0.5}O_2$ had already decreased to the final value of 11 $m^2\ g^{-1}$ after the initial thermal treatment, but we detected a high H/Pd ratio after reduction at 350 K. Since the bulk reduction/oxidation of ceria–zirconia mixed oxides induces significant reconstruction of the pore structure of the support (11), encapsulation of Pd on reduction at 473 K cannot be discounted. An alternative explanation is that the latter treatment simply blocks H_2 spillover from already partially encapsulated Pd particles to the support. Whatever the situation, in the TPR of fresh $Pt/Ce_{0.5}Zr_{0.5}O_2$ the high efficiency in H_2 activation coupled to a facile reduction of palladium oxide results in a low temperature for the first major peak.

In the recycled sample, Raman spectra indicate a strong oxygen sublattice modification as occurs in the Pt-loaded

sample. The combination of this effect and the low ability to activate H_2 move the support reduction up to 520 K. This temperature is slightly higher than that of Rh and Pt samples but significantly lower than those of both bare support and Rh/CeO_2.

The total degree of reduction of both unsupported and Rh-loaded CeO_2 is independent of sample history, i.e., fresh or recycled. Due to the CeO_2 surface area collapse, the ability to adsorb oxygen after low-temperature reduction is suppressed by the initial reduction up to 1273 K, which indicates the critical role of ZrO_2 in promoting OSC at low temperatures. This ability is present only in the fresh sample reduced at 700 K. Partial oxidation of Rh^0 to Rh^{3+}, which easily occurs at 700 K, may account for the apparent higher formation of oxygen vacancies in Rh/CeO_2 compared with CeO_2. Consistently, 0.04 mmol O_2 g^{-1} is calculated for the oxidation of Rh. Note that this amount is one order of magnitude smaller than the values reported in Table 1.

For $Ce_{0.5}Zr_{0.5}O_2$, a small decrease in oxygen uptake is observed during the first two runs, but after the second recycle, oxygen uptake is constant. The redox process in $Ce_{0.5}Zr_{0.5}O_2$ is more efficient than that in CeO_2 since about 50–60% of the cerium is reduced in the range 700–1273 K. Noticeably, the overall oxygen storage capacity does not depend on the presence of the supported metal. As long as a high reduction temperature is employed, the oxygen uptake is quite similar for all the NM-loaded and NM-free samples. Noteworthy is the unusually high efficiency of the Ce^{3+}/Ce^{4+} redox couple in the recycled $NM/Ce_{0.5}Zr_{0.5}O_2$ samples after strong sintering of the samples. In fact, in the case of recycled Rh- and Pt-loaded $Ce_{0.5}Zr_{0.5}O_2$, reduction at only 440 K yields an oxygen uptake of 90–80% of the overall OSC that decreases to 60% for Pd catalyst. At 600 K, the OSC of the recycled Rh/CeO_2 is nearly zero. Finally, it is remarkable that Pd achieves a high OSC even at a metal dispersion of only 5%.

Textural Properties

The stabilization of the surface area in the presence of supported rhodium is of interest. A tentative explanation may be related to the Sanchez and Gazquez (41) model of strong metal–support interaction for group VIII metals supported on reducible oxides. They suggested that noble metal can migrate over the oxide surface and may drop into the nests created by reduction/dehydroxylation. In this way, the metal atoms can be buried deep into the crystal structure of the support. Such a mechanism can easily interfere with the sintering process. In fact, SEM investigation of $Ce_{0.5}Zr_{0.5}O_2$, showed that the redox cycles induce a strong coarsening of the support via surface diffusion and/or vapor transport (11). Rhodium atoms buried in the fluorite lattice could interfere with the diffusion processes at the grain boundaries, increasing the thermal stability of the surface area of the support itself. The case of Pt- and Pd-loaded samples is different. The model proposed by Sanchez and Gazquez (41) suggests that metal burial may occur preferentially for relatively small metals, not much larger than the vacancy. The atomic radius of Rh (1.345 Å) is smaller than those of Pt (1.387 Å) and Pd (1.375 Å) (41), suggesting that Pt and Pd atoms might be too large to easily penetrate past the first cation layer of $Ce_{0.5}Zr_{0.5}O_2$, even in the presence of oxygen vacancies. Consistently Rh/CeO_2 shows SMSI, while Pt/CeO_2 does not (42).

CONCLUSIONS

The most important observation of the present work is the significant enhancement of the redox capacities of the Rh-, Pt-, and $Pd/Ce_{0.5}Zr_{0.5}O_2$ on thermal treatment. This result may represent an important breakthrough for the development of thermally stable TWCs. In fact, in CeO_2-based TWCs, the stability of the surface area is paramount, since the redox processes are essentially related to the surface at the typical temperatures of the converters. The results reported here clearly indicate that the oxygen storage capacity of the mixed oxide is unaffected by thermal sintering. This process is one of the most important pathways for the deactivation of TWCs.

Comparison of the microstructural properties of $NM/Ce_{0.5}Zr_{0.5}O_2$ with those of Rh/CeO_2 shows a parallel textural evolution on reduction/oxidation at high temperatures: the original pore structure is destroyed and new ones are formed due to the stresses and dislocations induced by the lattice contraction/expansion on oxidation/reduction. A significant decrease in BET surface area is observed. Rh interferes with the process of sintering of the support, preventing to some extent the collapse of the surface area. In contrast, Pt and Pd do not show similar ability.

The collapse of surface area strongly depresses all the low-temperature redox processes in Rh/CeO_2 while in $NM/Ce_{0.5}Zr_{0.5}O_2$, an improvement of reduction behavior is observed, giving a highly efficient low-temperature Ce^{4+}/Ce^{3+} redox couple.

ACKNOWLEDGMENTS

Professor Adriano Bigotto and Dr. Roberta Di Monte (University of Trieste) are acknowledged for helpful discussions. Ministero dell'Ambiente (Rome) and University of Trieste are acknowledged for financial support.

REFERENCES

1. Taylor, K. C., *in* "Catalysis-Science and Technology" (J. R. Anderson and M. Boudart, Eds.), Chap. 2. Springer-Verlag, Berlin, 1984.
2. Taylor, K. C., *Catal. Rev.-Sci. Eng.* **35**, 457 (1993).
3. Yao, H. C., and Yu Yao, Y. F., *J. Catal.* **86**, 254 (1984).
4. Harrison, B., Diwell, A. F., and Hallett, C., *Plat. Met. Rev.* **32**, 73 (1988).
5. Muraki, H., Shinjoh, H., Sobukawa, H., Yokota, K., and Fujitani, Y., *Ind. Eng. Chem. Prod. Res. Dev.* **24**, 43 (1985).

6. Usmen, R. K., Graham, G. W., Watkins, W. L. H., and McCabe, R. W., *Catal. Lett.* **30**, 53 (1995).
7. Bensalem, A., Bozon-Verduraz, F., Delamar, M., and Bugli, G., *Appl. Catal. A Gen.* **121**, 81 (1995).
8. Vidmar, P., Fornasiero, P., Kašpar, J., and Graziani, M., *J. Catal.* **171**, 160 (1997).
9. Zamar, F., Trovarelli, A., de Leitenburg, C., and Dolcetti, G., *J. Chem. Soc. Chem. Commun.*, 965 (1995).
10. Fornasiero, P., Di Monte, R., Ranga Rao, G., Kašpar, J., Meriani, S., Trovarelli, A., and Graziani, M., *J. Catal.* **151**, 168 (1995).
11. Fornasiero, P., Balducci, G., Di Monte, R., Kašpar, J., Sergo, V., Gubitosa, G., Ferrero, A., and Graziani, M., *J. Catal.* **164**, 173 (1996).
12. Fornasiero, P., Kašpar, J., and Graziani, M., *J. Catal.* **167**, 576 (1997).
13. Vis, J. C., van't Blik, H. F. J., Huizinga, T., van Grondelle, J., and Prins, R., *J. Catal.* **95**, 333 (1985).
14. Perrichon, V., Laachir, A., Abouarnadasse, S., Touret, O., and Blanchard, G., *Appl. Catal. A Gen.* **129**, 69 (1995).
15. Lieske, H., Lietz, G., Spindler, H., and Voelter, J., *J. Catal.* **81**, 8 (1983).
16. Choudhary, V. R., and Rane, V. H., *J. Catal.* **135**, 310 (1992).
17. Perrichon, V., Laachir, A., Bergeret, G., Frety, R., Tournayan, L., and Touret, O., *J. Chem. Soc. Faraday Trans.* **90**, 773 (1994).
18. Zotin, F. M. Z., Tournayan, L., Varloud, J., Perrichon, V., and Frety, R., *Appl. Catal. A Gen.* **98**, 99 (1993).
19. Bernal, S., Calvino, J. J., Cifredo, G. A., Gatica, J. M., Omil, J. A. P., and Pintado, J. M., *J. Chem. Soc. Faraday Trans.* **89**, 3499 (1993).
20. Bernal, S., Calvino, J. J., Cifredo, G. A., Rodriguez-Izquierdo, J. M., Perrichon, V., and Laachir, A., *J. Catal.* **137**, 1 (1992).
21. Fierro, J. L. G., Soria, J., Sanz, J., and Rojo, J. M., *J. Solid State Chem.* **66**, 154 (1987).
22. Tuller, H. L., and Nowick, A. S., *J. Electrochem. Soc.* **122**, 255 (1975).
23. Borer, A. L., Bronnimann, C., and Prins, R., *J. Catal.* **145**, 516 (1994).
24. Padeste, C., Cant, N. W., and Trimm, D. L., *Catal. Lett.* **28**, 301 (1994).
25. Sing, K. S. W., Everett, D. H., Haul, R. A. W., Moscou, L., Pierotti, R. A., Rouquerol, J., and Sieminiewska, T., *Pure Appl. Chem.* **57**, 603 (1985).
26. Harkins, W. D., and Jura, G., *J. Chem. Phys.* **11**, 430 (1943).
27. Barret, E. P., Joyner, L. G., and Halenda, P. P., *J. Am. Chem. Soc.* **73**, 373 (1951).
28. Yashima, M., Arashi, H., Kakihana, M., and Yoshimura, M., *J. Am. Ceram. Soc.* **77**, 1067 (1994).
29. Sayle, T. X. T., Parker, S. C., and Catlow, C. R. A., *J. Phys. Chem.* **98**, 13625 (1994).
30. McBride, J. R., Hass, K. C., Poindexter, B. D., and Weber, W. H., *J. Appl. Phys.* **76**, 2435 (1994).
31. Graham, G. W., Jen, H. W., Chun, W., and McCabe, R. W., *Catal. Lett.* **44**, 185 (1997).
32. Bernal, S., Botana, F. J., Calvino, J. J., Cauqui, M. A., Cifredo, G. A., Jobacho, A., Pintado, J. M., and Rodriguez-Izquierdo, J. M., *J. Phys. Chem.* **97**, 4118 (1993).
33. Bernal, S., Calvino, J. J., Cifredo, G. A., Laachir, A., Perrichon, V., and Herrmann, J. M., *Langmuir* **10**, 717 (1994).
34. Ragaini, V., Giannantonio, R., Magni, P., Lucarelli, L., and Leofanti, G., *J. Catal.* **146**, 116 (1994).
35. Di Monte, R., Kašpar, J., Fornasiero, P., Ferrero, A., Gubitosa, G., and Graziani, M., *Stud. Surf. Sci. Catal.* **116**, 559 (1998).
36. Vlaic, G., Fornasiero, P., Geremia, S., Kašpar, J., and Graziani, M., *J. Catal.* **168**, 386 (1997).
37. Balducci, G., Kašpar, J., Fornasiero, P., Graziani, M., and Islam, M. S., *J. Phys. Chem. B* **102**, 557 (1998).
38. Cunningham, J., Cullinane, D., Sanz, J., Rojo, J. M., Soria, J., and Fierro, J. L. G., *J. Chem. Soc. Faraday Trans.* **88**, 3233 (1992).
39. Bernal, S., Botana, F. J., Calvino, J. J., Cifredo, G. A., and Perezomil, J. A., *Catal. Today* **23**, 219 (1995).
40. Badri, A., Binet, C., and Lavalley, J. C., *J. Chem. Soc. Faraday Trans.* **92**, 1603 (1996).
41. Sanchez, M. G., and Gazquez, J. L., *J. Catal.* **104**, 120 (1987).
42. Meriaudeau, P., Dutel, J. F., Dufuax, M., and Naccache, C., *Stud. Surf. Sci. Catal.* **11**, 95 (1982).